

# Self-Folding Miniature Elastic Electric Devices

Shuhei Miyashita<sup>1,\*</sup>, Laura Meeker<sup>1</sup>, Michael T. Tolley<sup>2</sup>,  
Robert J. Wood<sup>2</sup>, and Daniela Rus<sup>1</sup>

<sup>1</sup> Computer Science and Artificial Intelligence Laboratory,  
Massachusetts Institute of Technology

<sup>2</sup> School of Engineering and Applied Sciences  
and the Wyss Institute for Biologically Inspired Engineering,  
Harvard University

\* corresponding author

32 Vassar Street, Cambridge, MA, 02139, USA  
shuheim@csail.mit.edu  
+1 412-228-8008

## Abstract

Printing functional materials represents a considerable impact on the access to manufacturing technology. In this paper we present a methodology and validation of print-and-self-fold miniature electric devices. Polyvinyl chloride laminated sheets based on metalized polyester film (MPF) show reliable self-folding processes under a heat application, and it configures 3D electric devices. We exemplify this technique by fabricating fundamental electric devices, namely a resistor, capacitor, and inductor. Namely, we show the development of a self-folded stretchable resistor, variable resistor, capacitive strain sensor, and an actuation mechanism consisting of a folded contractible solenoid coil. Because of their pre-defined kinematic design, these devices feature elasticity, making them suitable as sensors and actuators in flexible circuits. Finally, an RLC circuit obtained from the integration of developed devices is demonstrated, in which the coil based actuator is controlled by reading a capacitive strain sensor.

# 1 Introduction

The realization of “printing” functional robots has the potential to bring unprecedented wide-scale access to rapid and versatile fabrication of robotic artifacts. Recent progress in techniques for printing 3D structures has provided engineers with rapid prototyping of robotic structural components and consequently to robots development. The challenge now shifts toward printing entire robots - from sensing and actuation to controller to fully integrated and functional artifacts - with minimal human intervention. Toward this end, we develop a method and technique for self-assembling conductive materials to desired functional formations.

Recently, folding processes, inspired by Origami art work and protein folding, have been exploited for the construction of various types of robots. RoACH is a 2.4 g autonomous hexapod robot with a body shape made through folding and assembling processes [1]. Onal et al. developed inchworm robots by patterning a single Polyester sheet and manually folding [2]. Hawkes et al. achieved the self-folding of an origami structure using a shape memory alloy for actuation [3]. Yasu and Inami demonstrated the self-folding of a robot-like structure in a microwave oven, using a heat-sensitive sheet coupled with a microwave-sensitive aluminum sheet [4]. Felton et al. achieved the self-folding using Shape memory polymer powered by Joule heating, and showed an inchworm robot [5, 6]. Tolley et al. investigated various types of self-folding methods for robotic applications [7, 8], and Miyashita et al. achieved accurate self-folding of a robot’s structure based on Angle folds using global heating [9].

Whitney et al. developed  $\mu\text{m}$ -scale robots based on pop-up methods [10], and Abel et al. presented a theoretical framework for designing pop-up parallel folds [11]. Techniques for MEMS folding was shown in [12]. DNA origami was realized through one-dimensional structure folding in [13], and it was inspired by protein foldings in [14, 15, 16]. Elastomer-based folding techniques are presented in [17].

A different line of research focused on develop-

ing soft electronics providing versatile capabilities to stretch, compress, twist, bend, and deform [18, 19, 20, 21].

Toward the realization of “printable” robots, this paper investigates a method of print-and-fold that unifies structure and functionality for robot development. As such we present basic printable electric components and devices. The contribution of this study is developed based on [22], with additional exemplifications that the developed self-folding method is capable of producing miniature scale devices whose feature sizes scale down to the millimeter. The contributions of this paper are (1) a method for resistance, capacitance, and inductance through the use of a metalized polyester sheet, (2) a technique for self-folding and self-assembly of conductive material, (3) miniature devices (stretchable resistor, variable resistor, and capacitive strain sensor) as examples of self-folded functional electric devices and attained an origami-coil actuation mechanism, and (4) combined integration of these units in the form of a sensor-actuator system.

## 2 General Principles & Methods

Our technical approach for realizing resistors, capacitors, and inductors exploits the conductivity and resistivity using the structure or geometry of material sheets. In particular, we use  $50.1\ \mu\text{m}$  thick isotropic aluminum coating (one side) polyester film (Metalized Polyester Film, MPF).

A specific resistance can be attained by varying the material’s geometry. Thus, a  $3 \times 3\ \text{cm}$  square cut of MPF has about  $\approx 4.4\ \Omega$ . The resistance can be linearly increased by lengthening the MPF, and inversely, can be decreased by widening the width of the sheet. By translating this cutting-and-regulating approach to folding methods, we can realize elastic resistors of various resistances (the limit is given by the geometry).

Since the resistance of the MPF is relatively low (the sheet resistance  $\approx 1\ \Omega$ ), it can be used as

a conductive cable in short-length circuitry. The conductivity is not as high as that of copper, such a conductive cable is more suitable for digital circuits.

Capacitors can be obtained using two electrically isolated MPF. Capacitance of two parallel MPF is proportional to the surface area and inverse proportional to the distance between the plates. Thus, the capacitance magnitude can be regulated by the arrangement and the geometry of the paired surfaces. With folding, we realized a capacitor by pairing angled MPF surfaces, where a shared edge forms the hinge between the tiles. This way, for example, two square MPF of  $2 \times 2 \text{ cm}^2$  spanning an angle of  $45^\circ$  with a 2 mm gap from the shared edge exhibits a capacitance of  $\approx 0.4 \text{ pF}$ . Due to the fact that the capacitance increases roughly proportional to the surface area, the size of the device influences the capacitance magnitude.

Inductance is the resistivity of a structure against the current change, and is commonly seen in the form of a solenoid coil. To show the capability of self-assembly in realizing folded 3D structures that satisfy the topology of an inductor, we designed a self-folding solenoid coil. The coil can create a magnetic field within a certain volume, which can subsequently be used for actuation mechanisms, as introduced in Section 6.3. The inductance is determined by the number of turns as well as the geometry (size). For instance, an MPF solenoid coil with radius 16 mm, height 6 mm, and 5 turns theoretically has an inductance of  $2.10 \mu\text{H}$ .

Tests with an MPF-based inductor showed that it can sustain up to an  $\approx 300 \text{ mA}$  current before an instant loss of conductivity occurs due to changes in the characteristic of the polyester layer produced by heat. MPF maintains conductivity as well as resistivity given the non-harsh iterative foldings. The sheet can withstand a temperature range of  $-45^\circ\text{C}$  to  $148^\circ\text{C}$ , making the material a poor candidate for soldered connections. Therefore, conductive connections in the circuit were made using conductive tape, conductive epoxy glue, and mechanical clippings.

### 3 Self-folding Method of MPF

#### 3.1 Global Heating Application and Three Layer Structure

Among the various existing self-folding techniques, we have developed a simultaneous multi-crease self-folding technique based on global heating with a heat sensitive sheet (Poly-Vinyl Chloride; PVC, Shrink Bag, shrinking temperature:  $65^\circ\text{C} \sim 75^\circ\text{C}$ , thickness 0.025 mm) [9]. The key insight is to transform the internal stress of a contraction sheet into a folding torque. Our goal is to globally heat the structure to induce simultaneous foldings. Fig. 1 shows the designed mechanism for self-folding. The

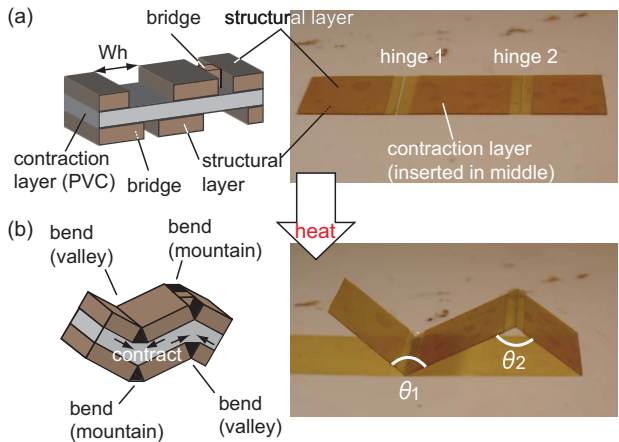


Figure 1: Proposed self-folding method using global heating.

PVC contraction layer is sandwiched by non-deformable structural layers with different gap widths. When the structure is heated, the shear force disproportionates to one side and generates a bending torque (Fig. 1 (a),(b)). The gap width difference between the front and back of the sheet at the same position enables the differentiation of the bending direction: the planes bend toward wider gaps. The approach is capable of folding mountain and valley folds simultaneously. Furthermore, the folding angle ( $\theta_1$  and  $\theta_2$  in Fig. 1) can be approximately encoded with the gap widths as well as the bridge width. Namely, the wider  $W_h$ , the steeper the folding angle becomes. The designs presented in this work feature Angle folds, which enables precise

targeted folding angles by indirectly actuating other folding angles that are kinematically coupled (see [9]).

PVC has two ideal features: the capability of low temperature contraction (less than 100 °C), and a relatively robust physical structure with transparent visibility. PVC also has some disadvantages: the material may deform at high room temperature, and it cannot be cut with a laser machining system due to the emission of toxic gases.

### 3.2 Fabrication

Fig. 2 shows the design and fabrication process. After determining the desired variable properties, such as the folded sheet structure, kinematics, and circuit topology, we derived the crease pattern for self-folding considering all conditions (Fig. 2 (a)→(b)). The unique characteristics of this approach are: (1) alignment of the laminated three layers is achieved with a single fold during fabrication (Fig. 2(d)); (2) the geometry of the target 3D structure (Fig. 2(a)) can be encoded in the folding pattern (Fig. 2(b)) to be realized after self-folding (Fig. 2(f)); (3) there are driving (or input) angles and driven (output) angles, and the accurate driven angles are roughly controlled by the driving angles by balancing out the torsion by bridges with generated torque (Fig. 2(f)); (4) with the exception of the laser machining during fabrication, the entire process is completed without the assistance of equipment; (5) the conductive surface in the self-folded 3D structure can be exposed or hidden depending on which side of the MPF faces up in the lamination phase (Fig. 2(c)); (6) further lamination of layers is possible to provide additional functionalities.

Conductivity is maintained via “bridges” that link the conductive tiles (Fig. 2(c)), which also maintain a constant separation between tiles during self-folding and enforce the direction of folds. (Due to the torque required, bridges can only be placed over mountain folds). The total thickness of the self-folding sheet is 0.3 mm.

## 4 Resistance

### 4.1 Model

This section models the MPF resistor. For 3D resistance,  $R = \frac{\rho}{l_t} \frac{l_h}{l_w} := R_s \frac{l_h}{l_w}$ , where  $\rho$  is the resistivity intrinsic to the material,  $l_t$  is the unknown thickness of coated aluminum,  $l_h$  is the height,  $l_w$  is the width of the material, and  $R_s$  is the sheet resistance. We measured the resistivity of the material using the Van der Pauw method (the sample thickness is much less than the width and length of the sample [23]), and obtained the sheet resistance of  $R_s = 0.933 \Omega$ .

Fig. 3 shows the plot of experimentally measured resistances depending on the different width ( $l_w$ ) to height ( $l_h$ ) ratios of the rectangular MPF. By fitting the curve, we obtain  $R =$

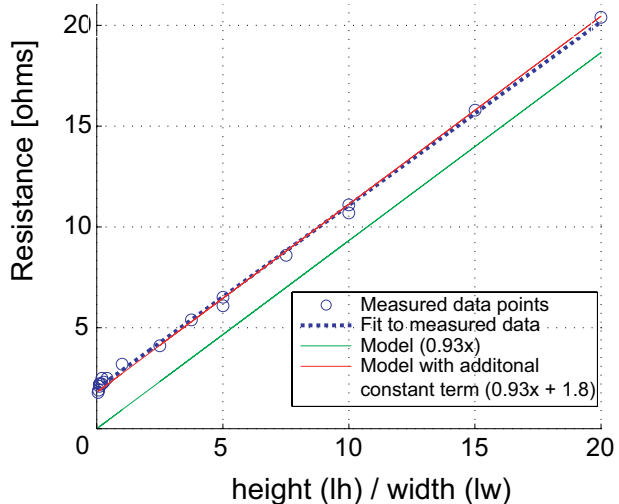


Figure 3: Resistance of MPF with different geometries.

$0.93 \frac{l_h}{l_w} + 1.8$ , which shows a similar value to what we obtained from the Van der Pauw method, and we will use this model for rectangular resistors.

To embed resistance within a (self-)folded structure, we wish to estimate the resistance when bridges are included in a pattern (see Fig. 2). Fig. 4 illustrates various resistances made by cutting  $3 \times 3 \text{ cm}^2$  pieces of MPF and varying the width ( $l_w$ ) and height ( $l_h$ ) of the bridges. By comparing (b) and (h), it can be derived that the position of a bridge does not affect the resistance. The resistance of a sheet,  $R_{total}$

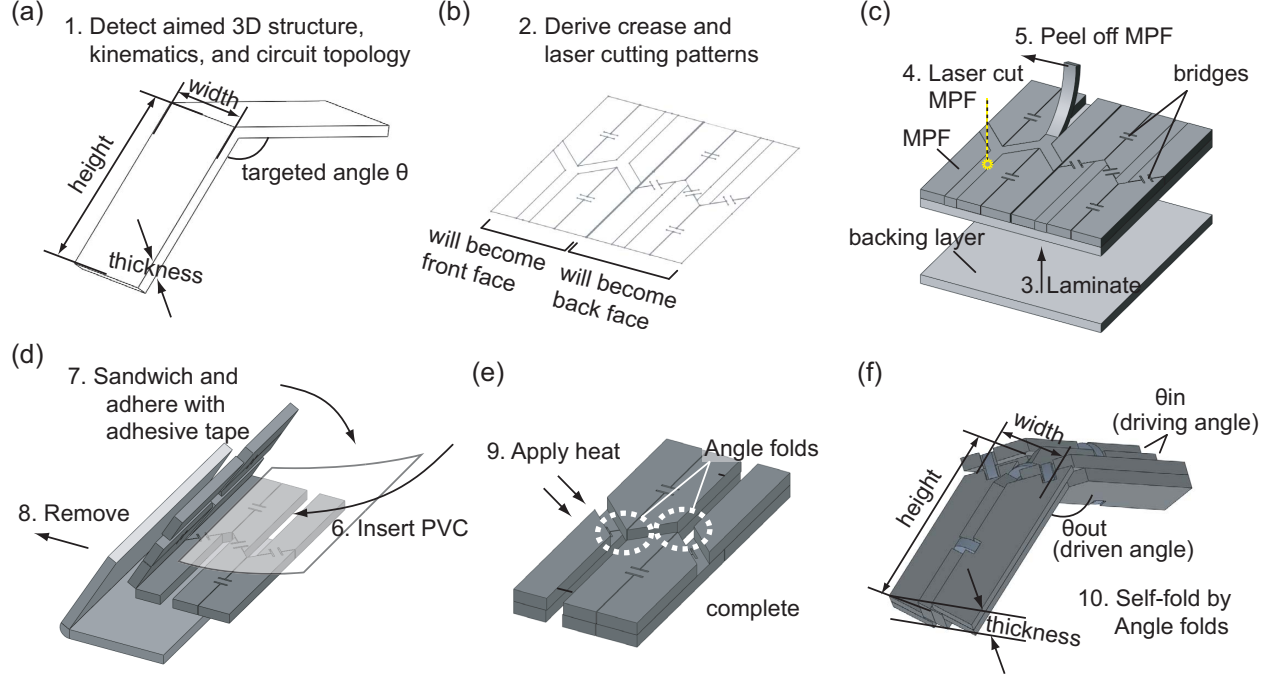


Figure 2: Design, fabrication, and self-folding processes.

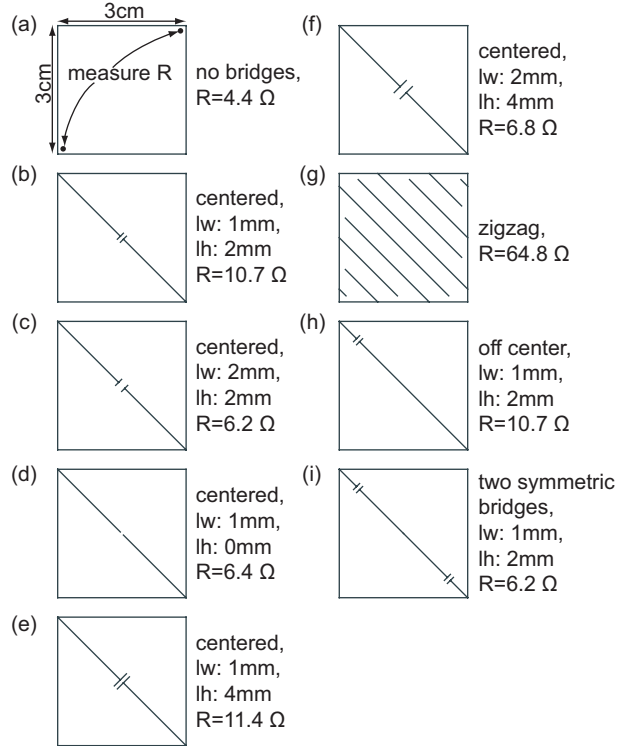


Figure 4: Various resistances realized by cutting  $3 \times 3 \text{ cm}^2$  MPF.

can be modeled as connections of the  $i$ -th ( $i \in \mathbb{N}$ ) surfacial geometric portion that attributes the resistance  $R_i$  connected in parallel and in series. For example, the resistance  $i$  serial resistances, each composed of one surfacial portion, can be calculated as  $R_{total} = \sum_i R_i$  where  $R_i$  is the resistance of the  $i$ -th surface. For example, the total resistance of the structure in Fig. 4 (b) can be approximately calculated as the sum of the resistance of Fig. 4 (d) and the  $1 \times 2 \text{ mm}^2$  bridge portion. With this model, our calculation estimates that the  $R_{total}$  of Fig. 4 (b) is  $10.18 \Omega$ , while the measured value was  $10.7 \Omega$  ( $\approx 5.1\%$  error). In the same way, the model estimates the  $R_{total}$  of Fig. 4 (e) as  $12.0 \Omega$ , where the measured value was  $11.4 \Omega$  ( $\approx 5.0\%$  error). Considering that the measured resistances are relatively small and are not stable when measured with a multimeter, the derived model can be considered to reasonably estimate the model. In practice, with a surface area  $3 \times 3 \text{ cm}^2$ , our estimation of the achievable resistance range is  $\approx 4 \Omega - 3.2 \text{ k}\Omega$ , with the assumption that the thinnest width obtainable with our laser cutter is  $l_w = 0.5 \text{ mm}$ . This resolution and the layer alignment accuracy

mainly limit the attainable smallest feature size to be at the mm-scale.

## 4.2 Stretchable resistor

Fig. 5 shows one of the images of self-folded resistor (MPF resistor). In order for the resistor to attain physical compressibility and stretchability in one direction, we combined slit traces [24] and Angle folds (Fig. 5(a)). The result is a structure with reversible extension ratios of up to 118 with the large scale model, and 5 with the small scale model (the difference is due to the fact that the thickness of the material is constant).

Fig. 5(b) shows the self-folding process. 68 creases are simultaneously folded in about 2 minutes after the initiation of deformation. Deformation occurs at temperatures over  $50^{\circ}\text{C}$  (the oven requires approximately 2 minutes to reach this temperature). In general, the duration depends on the characteristic of the oven used, though a steady increase in temperature is required to keep spatial uniformity in self-folding.

The structure is floated on water during the process in order to avoid direct heat application and to reduce the frictional influence of ground when deformation occurs. We note that self-folding can be attained also on a low-frictional surface such as Teflon sheet. With gradual heating, the temperature of the water to be approximately the same as the air temperature in the oven during self-folding experiments.

We show the self-folded MPF resistor in Fig. 5(c), with a 5 : 1 scale model fabricated with the same process in Fig. 5(d).

## 4.3 Variable resistor

This section demonstrates self-folding of a variable resistor as a demonstration of the capabilities of our system. The idea was to connect the electrical tiles that make up a folded structure in an electrical circuit, and to manually short the circuit, thereby changing (reducing) the resistance in steps (four steps in this case). The tiling pattern and the path of electrical conductivity (depicted with blue lines) are shown in Fig. 6(a). This figure shows tiles from the front surface in

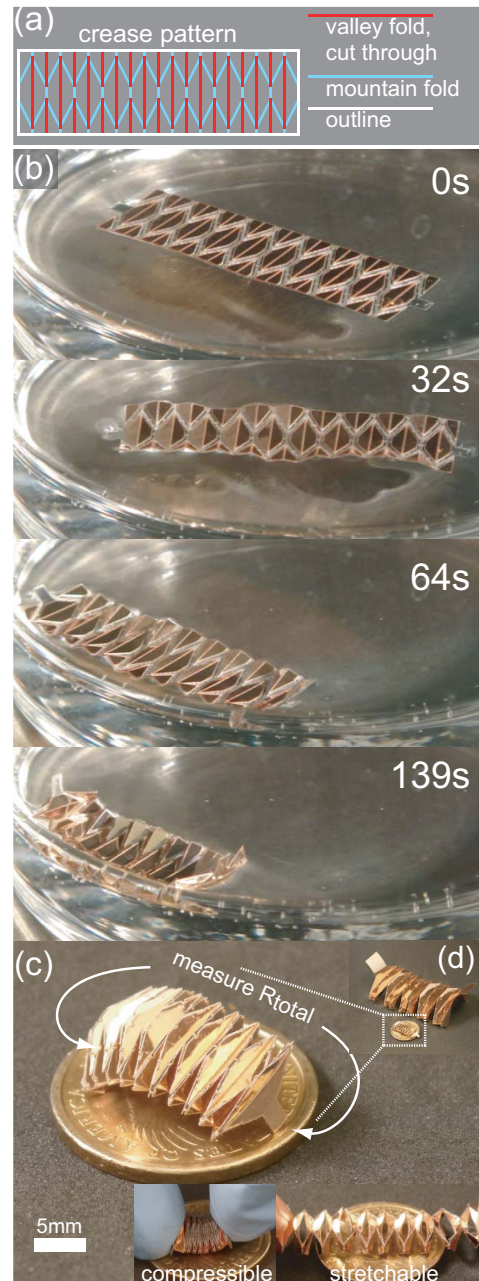


Figure 5: Designed stretchable/compressible MPF resistor. (a) The crease pattern. (b) Self-folding process. (c) Self-folded MPF resistor at normal length with compressed and stretched images besides (US dollar coin included for scale). (d) Large scale self-folded MPF using the same fabrication process. Highlighted with square is magnified in (c). See the self-folding process in the supplemental video.

red and from the back surface in blue. This circuit topology allows for adjacent faces to be electrically connected in series, and the self-folded 3D geometry forms a scaling zigzag pattern for easy pinching to vary the measured resistance. Fig. 6 (b) shows images from self-folding experi-

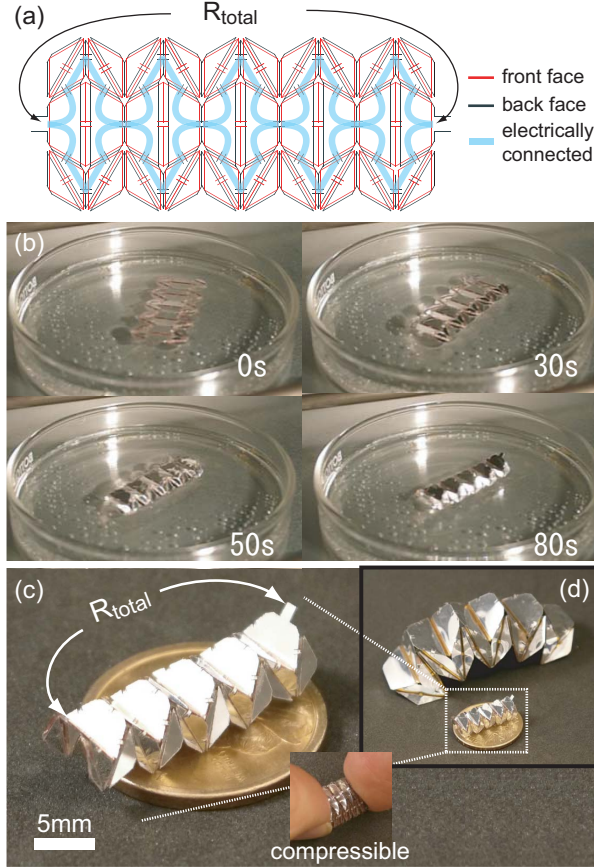


Figure 6: Self-folded MPF variable resistor. (a) Designed crease pattern with front and back sides overlaid. (b) Self-folding process in an oven. (c) The outlook of the self-folded variable resistor and the compressed and stretched states in the insets. (d) Two-shot image with larger scale variable resistor generated with the same technique. See the self-folding process in the supplemental video.

ments. The repeatable self-folding process took about one and a half minutes after the deformation initiated. Fig. 6 (c) shows the self-folded MPF variable resistor. Due to the kinematics of the structure, linearly aligned tiles on the top

surface can be shorted by hand, as shown in the inset. The structure possesses elasticity, and it recovers its original posture when the external force is removed.

For reliable output values, we tested the large scale variable resistor. The measured resistances are  $83.56 \pm 1.44 \Omega$  (with no pinches),  $74.48 \pm 2.20 \Omega$  (with 1 of 4 sections pinched),  $62.49 \pm 1.86 \Omega$  (2 pinches), and  $49.94 \pm 0.94 \Omega$  (3 pinches) (in each case,  $n = 8$ ). By approximating triangular shapes to the similar geometric ratios' rectangles, our model roughly estimates the resistance with no pinches as  $\approx 90.4 \Omega$ . Due to limitations of our CO<sub>2</sub> laser machining system we used, the actual dimensions of the bridges do not reliably reproduce the intended designs.

## 5 Capacitance

### 5.1 Model

In order to fabricate capacitors by self-folding, we explored designs composed of electrically isolated conductive faces, mechanically connected along fold edges. Here we develop an analytical model for the fundamental case of identically shaped paired angled MPF tiles (see Fig. 7 for the schematic representation of a side view in (a) and an angled view in (b)). Each capacitor is made up of two conductive isosceles triangular tiles (colored in red). Here,  $r$  is the length of the non-conducting parts of the upper and lower tiles measured from their common hinge, respectively, and  $l$  is the height of the aluminum coated conductive part of respective conductive surfaces ( $\therefore r + l \leq \text{height of tile}$ ).

The thickness of the tiles, 0.05 mm, is denoted as  $\frac{T}{2}$ , and the angle of the outward facing tip of each tile is given by  $\phi$ . The capacitance of the tile pair varies in accordance with the relative angle between them, which is given by  $\theta$ . Defining the x-axis as parallel to the bottom face, the capac-

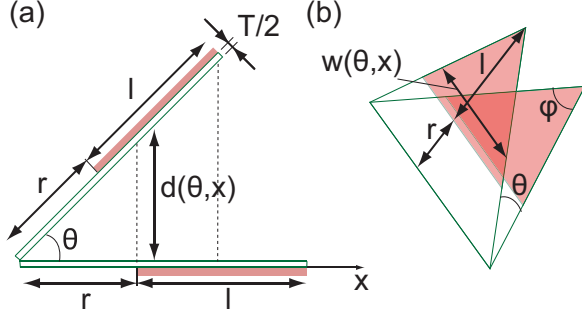


Figure 7: Capacitor for a folding structure. Schematics in a side view (a) and in an angled view (b). Conductive portions are shown in red.

itance  $C$  as a function of angle  $\theta$  is:

$$\begin{aligned}
 C(\theta) &= \epsilon_0 \epsilon_r \int_r^{r+l} \frac{w(\theta, x)}{d(\theta, x)} dx \\
 &= \frac{\epsilon_0 \epsilon_r \tan \frac{\phi}{2}}{\tan \theta} \\
 &\left( (r+l) \ln \left( \frac{(r+l) \cos \theta}{r} - (r+l) + \frac{r}{\cos \theta} \right) \right), \quad (1)
 \end{aligned}$$

where  $\epsilon_0 = 8.85 \times 10^{-12} \text{ Fm}^{-1}$  and  $\epsilon_r = 1.00059$  are the absolute permittivity and relative permittivity of air, respectively,  $w(\theta, x)$  is the width of the conductive plate, and  $d(\theta, x)$  is the distance between the two plates at position  $x$ .

## 5.2 Capacitive strain sensor

Based on the folded capacitor model described in the previous section, we produced a self-folding capacitive strain sensor. The crease pattern, shown in Fig. 8(a), was developed based on the X-form spans folding pattern [25]. The tiling pattern with connections between tiles via bridges formed a compressible five parallel capacitors when self-folded, and thus could be used as a capacitive strain sensor. Using global heating in an oven, the sheet reliably activated 100 creases simultaneously and self-folded into the intended 3D strain sensor (Fig. 8(b)). Note that all the necessary circuitry was defined during laser machining, thus the structure was ready to use after self-folding. Due to the kinematics

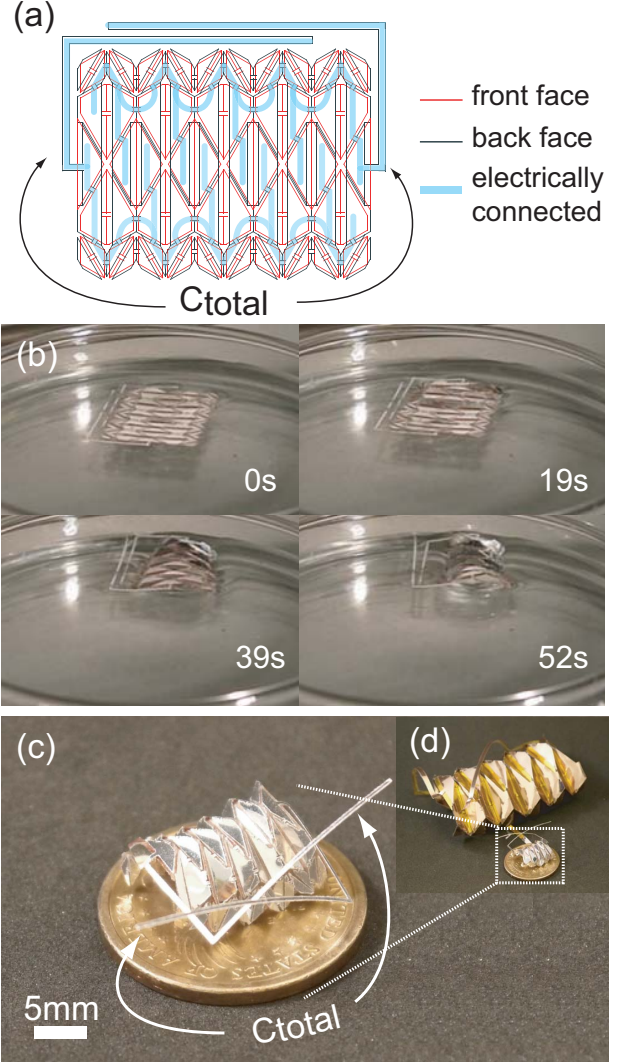


Figure 8: Self-folding of a capacitive strain sensor made in an oven. See the self-folding process in the supplemental video.

of the structure, it can be compressed, and when the force was released, the structure expanded back to its original length.

We measured the capacitance of our strain sensor as a function of the applied strain (Fig. 9). Within the marked region of  $30 - 60^\circ$ , the sensor showed approximately linear behavior according to the equation  $C_{total} = 11.67 \cdot \text{strain} + 12.01$ . Within this region, the measured resistance increased by 15% with respect to its original value, making it a functioning capacitive strain sensor.

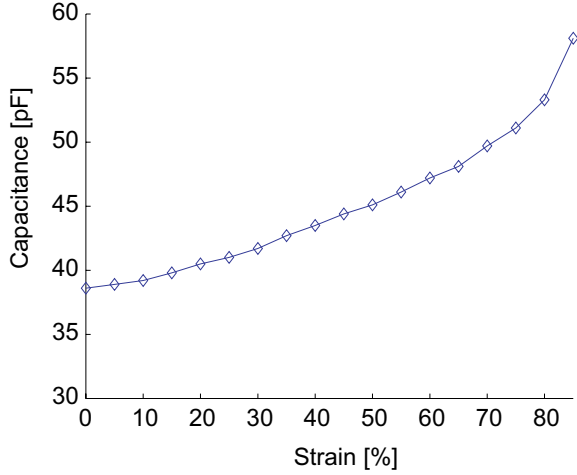


Figure 9: Capacitance of self-folded strain sensor.

## 6 Inductance

### 6.1 Model

To generate an accurate model for folded inductive coils, we employed Harold Wheeler’s formula [26] for calculating the inductance,  $L$ , of a single-layer coil since this formula smoothly connects the “short coil” and “long coil” approximations:

$$L = \mu_0 n^2 l_R \left[ \ln \left( 1 + \frac{\pi l_R}{l_H} \right) + \left( 2.3 + 1.6 \left( \frac{l_H}{l_R} \right) + 0.44 \left( \frac{l_H}{l_R} \right)^2 \right)^{-1} \right], \quad (2)$$

where  $\mu_0$  is the permeability of free space,  $n$  is the number of turns,  $l_R$  is the radius of the coil, and  $l_H$  is the height of the coil.

First, we determined the crease pattern for self-folding (Fig. 10(a)). The folding pattern was designed to (1) generate a spiral structure of six folds per coil turn, (2) attribute a determinate thickness to the wire for stable overlap, and (3) electrically connect all the tiles for current flow along the spiral structure. The entire pattern was designed to configure into a hexagonal coil of 5 turns, 16.0mm radius, and a height of 6.0mm. Note that the helix radius of this design (and thus the density of turns and coil height)

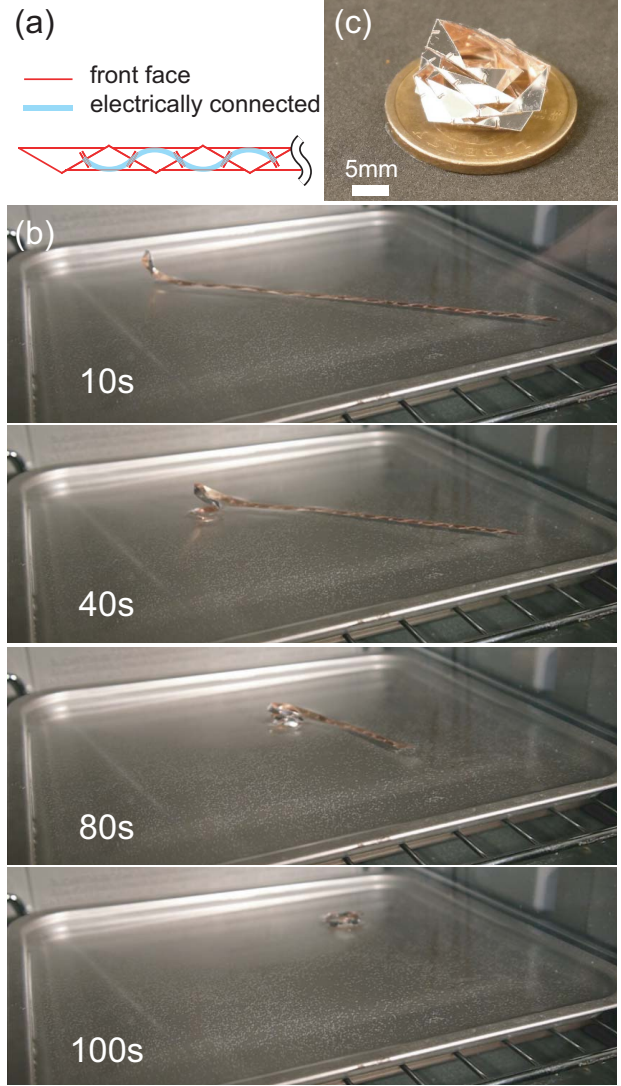


Figure 10: Self-folding MPF coil: (a) crease pattern, (b) self-folding process, and (c) MPF solenoid coil. See the self-folding process in the supplemental video.

can be adjusted by regulating the gap widths of the valley. As the folding angle approaches  $180^\circ$ , the turn density reaches its maximum value and the magnetic field increases for a given current.

### 6.2 Solenoid coil

Fig. 10(b) shows the self-folding process of the MPF solenoid coil. The folding, from beginning to end, only took about a minute and a half. Fig. 10(c) shows the self-folded solenoid

coil. Note that due to the kinematics, the coil could be compressed. Wheeler’s formula predicted  $L = 0.52 \mu\text{H}$ , though the actual value was too small to measure with an LCR meter.

### 6.3 Application to Actuation Mechanism

In order to demonstrate the effect of the magnetic field generated by a folded solenoid coil, we investigated the possibility of an actuation mechanism. The basic design was based on a voice coil, in which an electrical coil generates a force that acts on a permanent magnet, vibrating a membrane to generate sound. Our approach was to have a compressible origami coil with two ferrous cylindrical cores suspended inside both ends. When the current was run through the coil, the ferrous cores within become magnetized in the same direction and attracted each other (Fig. 11 (a)). The coil would then contract due to the attractive force between the ferrous cores. A similar concept is used in microrobotics to achieve locomotion in a microrobot equipped with two magnets, the separation of which are manipulated using an externally applied resonant magnetic field [27].

In practice, our conductive material (MPF), was unable to conduct sufficient current for actuation at this scale. We therefore utilized a manually folded 24-winding copper-based origami coil with the same folding geometry pattern shown in Fig. 10. In this case we insulated the copper layers using polyimide tape. For the cores, we

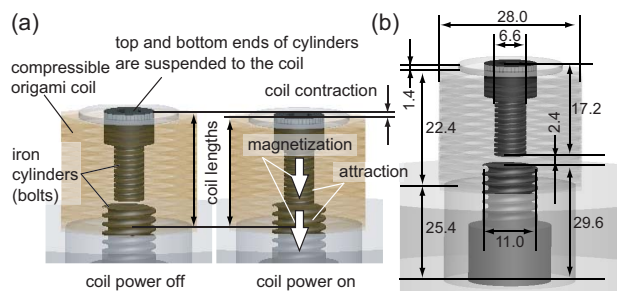


Figure 11: Concept and schematics of origami-coil actuation mechanism. Units are in mm.

used a 6.3 mm diameter ferrous cylinder (bolt)

for the upper end and an 11.1 mm diameter ferrous cylinder for the lower end. Using an LCR meter, we measured the inductance of this folded coil to be  $L = 4.6 \mu\text{H}$ , which was 8% smaller than the value predicted by Wheeler’s formula ( $L = 5.0 \mu\text{H}$ ).

Fig. 12 shows the magnetic flux density generated by the origami coil, which increased as a linear function of the applied current.

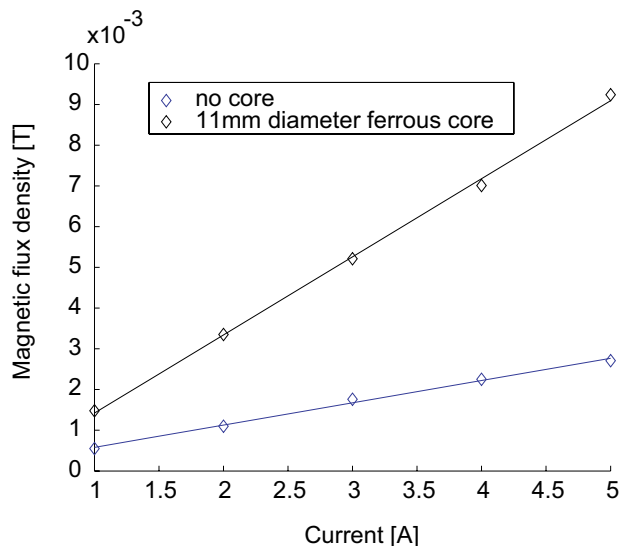


Figure 12: Magnetic field density generated by manually folded copper origami coil.

We tested the origami voice coil actuator by applying current and measuring the resulting contraction caused by attraction of the magnetized cores (Fig. 12). At 5 A of applied current, a  $\approx 0.8 \text{ mm}$  contraction ( $\approx 3.57\%$  compression) was observed in the structure. Presumably, the amount of contraction could be improved using a thinner insulation layer, a larger number of coil windings, or a higher application of current. The non-linear increase of contraction with applied current results from the nonlinear strength of the magnetic force between the cores, which is inversely proportional to their relative separation to the power of four. While predicting the compression rate to obtain a precise model of the spring constant of our origami coil is required for further development of this actuator, we leave this characterization for future work.

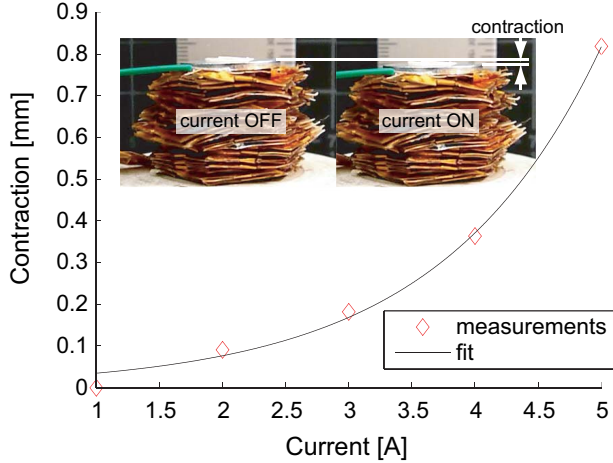


Figure 13: Contraction measured with different current amounts.

## 7 Integration of Devices

This section demonstrates the integrated use of the three electric devices presented above; namely, the self-folded MPF resistor, the self-folded MPF capacitive strain sensor, and the manually folded origami-coil actuator. We read

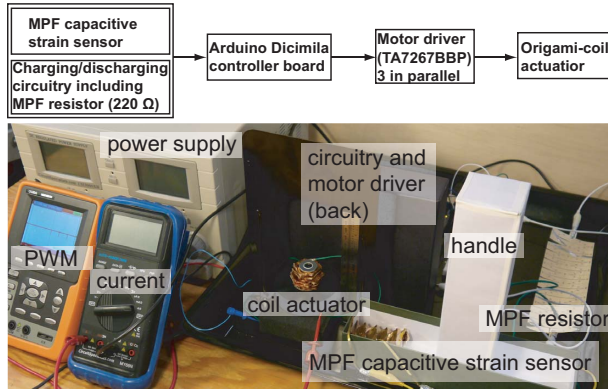


Figure 14: Experimental setup and control diagram. The demonstration is shown in the supplemental video.

the (large scale) MPF capacitive strain sensor data with an Arduino controller board with the support of two resistors ( $10\text{ M}\Omega$  and  $220\ \Omega$ ), and we controlled the magnetic field strength generated by the folded-coil actuator as the linear output of the strain value of the (large scale) MPF capacitive strain sensor. We incorporated the MPF resistor into the circuit as the  $220\ \Omega$  resis-

tor. A range of 10 to 50 pF of optimized capacitance, regulated manually through compression, is linearly mapped to a 0 to 5 A current range in order to power the origami-coil actuator. Fig. 14 shows the experimental setup and the control diagram. With the compression of the capacitive strain sensor, we observed the compression of the origami-coil actuator resulting from the generation of a magnetic field from the origami-coil. The demonstration, which is shown in the supplemental video, demonstrates the combined usage of the devices presented in this paper.

## 8 Discussion & Conclusion

In this paper, we presented the method, development, and usage of self-folding electric devices. We combined MPF and a heat-sensitive shrinking film to fabricate self-folding structures activated by applying global heating. The resulting folded structures are characterized by both conductivity and elasticity, making this approach appropriate for the fabrication of elastic electric devices, such as a variable resistor, a strain sensor, and a voice-coil based actuator. The result indicates that the required circuit topology can co-exist with the capability of self-folding while satisfying the required kinematics for the sensor. We further integrated these devices and demonstrated basic sensor-motor control by reading the strain of the capacitive sensor and regulating the folded coil-based actuator.

The novel electric devices have unique properties due to the underlying material and the fabrication process. The MPF resistors have limitations in terms of the maximum resistance output when compared to conventional resistors. Nonetheless, the structure features elasticity and tangibility in fabrication. The maximum value of the MPF capacitor is in the pF range. This implies that an appropriate use for these capacitors is as sensors, as they showed reliable and repeatable outputs. The limited current capacity that the MPF coil supports is not a negligible issue, but it will be addressed in future work in order to create actuation mechanisms with higher output.

In summary, the methodology showed the potential of using a conductive polyester sheet for electric devices by means of a simple and cheap printing-based fabrication and a reliable self-folding process. In addition to pursuing the creation of a wide functional platform based on the presented methodology, future work will continue to improve the automation of the entire process.

## Acknowledgment

Support for this work has been provided partially by NSF grants 1240383 and 1138967, and the Swiss National Science Foundation Fellowship Grant PBZHP2-133472.

## References

- [1] Hoover M A, Steltz E and Fearing S R 2008 RoACH: An autonomous 2.4g crawling hexapod robot *IEEE/RSJ International Conference on Intelligent Robots and Systems (IROS)*
- [2] Onal D C, Wood J R and Rus D 2011 Towards printable robotics: Origami-inspired planar fabrication of three-dimensional mechanisms *IEEE International Conference on Robotics and Automation (ICRA)*
- [3] Hawkes E, An B, Benbernou M N, Tanaka H, Kim S, Demaine D E, Rus D and Wood J R 2010 Programmable matter by folding *Proceedings of the National Academy of Sciences*, **107** 12441–12445
- [4] Yasu K and Inami M 2012 Popapy: instant paper craft made up in a microwave oven *The 9th International Conference on Advances in Computer Entertainment*
- [5] Felton M S, Tolley T M, Shin B-H, Onal D C, Demaine D E, Rus D and Wood J R 2013 Self-folding with shape memory composites *Soft Matter*, **9** 7688–7694
- [6] Felton M S, Tolley T M, Onal D C, Rus D and Wood J R 2013 Robot self-assembly by folding: A printed inchworm robot *IEEE International Conference on Robotics and Automation (ICRA)*
- [7] Tolley T M, Felton M S, Miyashita S, Xu L, Shin B-H, Zhou M, Rus D and Wood J R 2013 Self-folding shape memory laminates for automated fabrication *IEEE/RSJ International Conference on Intelligent Robots and Systems (IROS)*
- [8] Tolley T M, Felton M S, Miyashita S, Aukes D, Rus D and Wood J R in press Self-folding origami: shape memory composites activated by uniform heating *Smart Materials and Structures*
- [9] Miyashita S, Onal D C and Rus D 2013 Self-pop-up cylindrical structure by global heating *IEEE/RSJ International Conference on Intelligent Robots and Systems (IROS)*
- [10] Whitney P J, Sreetharan S P, Ma K and Wood J R 2011 Pop-up book MEMS *Journal of Micromechanics and Microengineering*, **21** 115021
- [11] Abel Z, Demaine D E, Demaine L M, Eisenstat S, Lubiw A, Schulz A, Souvaine L D, Viglietta G and Winslow A 2013 Algorithms for Designing Pop-Up Cards In Nat-acha Portier and Thomas Wilke, editors, *30th International Symposium on Theoretical Aspects of Computer Science (STACS 2013)*, volume 20 of *Leibniz International Proceedings in Informatics (LIPIcs)*, pages 269–280, Dagstuhl, Germany
- [12] Bassik N, Stern M G and Gracias H D 2009 Microassembly based on hands free origami with bidirectional curvature *Applied Physics Letters*, **95** 091901–1–091901–3
- [13] Rothmund K W P 2006 Folding DNA to create nanoscale shapes and patterns *Nature*, **440** 297–302
- [14] Clark D T, Boncheva M, German M J, Weck M and Whitesides M G 2001 Design of three-dimensional, millimeter-scale models

- for molecular folding *Journal of the American Chemical Society*, **124** 18–19
- [15] Saul Griffith 2004 *Growing Machines*. PhD thesis, MIT
- [16] Cheung C K, Demaine D E, Bachrach R J and Griffith S 2011 Programmable assembly with universally foldable strings (moteins) *IEEE Transactions on Robotics*, **27** 718–729
- [17] Martinez V R, Fish R C, Chen X and George M. Whitesides 2012 Elastomeric origami: Programmable paper-elastomer composites as pneumatic actuators *Advanced Functional Materials*, **22** 1376–1384
- [18] Rogers A J, Someya T and Huang Y 2010 Materials and mechanics for stretchable electronics *Science*, **327** 1603–1607
- [19] Kim R-H, Kim D-H, Xiao J, Kim B-H, Park S-I, Panilaitis B, Ghaffari R, Yao J, Li M, Liu Z, Malyarchuk V, Kim D-G, Le A-P, Nuzzo G R, Kaplan L D, Omenetto G F, Huang Y, Kang Z and Rogers A J 2010 Waterproof AlInGaP optoelectronics on stretchable substrates with applications in biomedicine and robotics *Nature materials*, **9** 929–937
- [20] Kaltenbrunner M, Sekitani T, Reeder J, Yokota T, Kuribara K, Tokuhara T, Drack M, Schwödiauer R, Graz I, B-G S, Bauer S and Someya T 2013 An ultra-lightweight design for imperceptible plastic electronics *Nature*, **499** 458–463
- [21] Kim D-H, Ahn J-H, Choi M W, Kim H-S, Kim T-H, Song J, Huang Y Y, Liu Z, Lu C and Rogers A J 2008 Stretchable and foldable silicon integrated circuits *Science*, **320** 507–511
- [22] Miyashita S, Meeker L, Göldi M, Kawahara Y and Rus D 2014 Self-folding printable elastic electric devices: Resistor, capacitor, and inductor *IEEE International Conference on Robotics and Automation (ICRA)*
- [23] Van der Pauw J L 1958 A method of measuring specific resistivity and hall effect of discs of arbitrary shape Technical Report 13, Philips Research Reports
- [24] Paik K J, Kramer K R and Wood J R 2011 Stretchable circuits and sensors for robotic origami *IEEE/RSJ International Conference on Intelligent Robots and Systems (IROS)*
- [25] Jackson P 2011 *Folding Techniques for Designers From Sheet to Form* Laurence King Publishing Ltd
- [26] Wheeler A H 1982 Inductance formulas for circular and square coils *Proceedings of the IEEE*, **70** 1449–1450
- [27] Frutiger R D, Vollmers K, Kratochvil E B and Nelson J B 2009 Small, fast, and under control: wireless resonant magnetic micro-agents *International Journal of Robotics Research*, **13** 1–24